Earth and Planetary Science Letters 362 (2013) 283–293

Contents lists available at SciVerse ScienceDirect

Earth and Planetary Science Letters

journal homepage: www.elsevier.com/locate/epsl

Reduced, reused and recycled: Detrital zircons define a maximum age for the Eoarchean (ca. 3750–3780 Ma) Nuvvuagittuq Supracrustal Belt, Québec (Canada)

Nicole L. Cates[a], Karen Ziegler[b,c], Axel K. Schmitt[b], Stephen J. Mojzsis[a,d,*]

[a] Department of Geological Sciences, University of Colorado, 2200 Colorado Avenue, UCB 399, Boulder, CO 80309-0399, USA
[b] Department of Earth and Space Sciences, University of California, 595 Charles Young Drive East, Box 951567, Los Angeles, CA 90095-1567, USA
[c] Institute of Meteoritics, University of New Mexico, 221 Yale Boulevard NE, 313 Northrup Hall, Albuquerque, NM 87131, USA
[d] Laboratoire de Géologie de Lyon, Université Claude Bernard Lyon 1, Ecole Normale Supérieure de Lyon, CNRS UMR 5276, 2 rue Raphaël DuBois, Bât. Géode 3e, Villeurbanne, France

ARTICLE INFO

Article history:
Received 7 April 2012
Received in revised form
26 November 2012
Accepted 28 November 2012
Editor T. Elliot
Available online 16 January 2013

Keywords:
Eoarchean
Nuvvuagittuq
quartzite
zircon
geochronology
detrital

ABSTRACT

A key discovery from the Hadean (pre-3850 Ma) detrital zircon record has been that the dichotomy of granitic and basaltic crust was established within about 160 Myr of Earth's formation (Harrison, 2009). Understanding the origin and fate of this primordial crust would greatly add to what we know about the geodynamics of the Hadean Earth. Insights emerge from ^{147,146}Sm–^{143,142}Nd isotope data reported from different Eoarchean terranes worldwide, including the Nuvvuagittuq Supracrustal Belt (NSB) in northern Québec. Some Ca-poor (cummingtonite-rich) amphibolites and granitoid gneisses of the NSB preserve lower ^{142}Nd/^{144}Nd than Bulk Silicate Earth (BSE); these also show positive correlations against ^{147}Sm/^{144}Nd that were used by O'Neil et al. (2008, 2012) to assign a ca. 4400 Ma age. Alternatively, the compositions were inherited during the formation of the NSB at around 3800 Ma (Roth et al., 2013; Guitreau et al., 2013). To resolve this discrepancy, ion microprobe U–Pb ages are reported for detrital zircons from NSB meta-sediments from within the same supracrustal successions that preserve low ^{142}Nd/^{144}Nd. The youngest detrital zircon cores of igneous derivation define a maximum age for the NSB of ca. 3780 Ma. This age is about 600 Myr younger than that obtained from ^{142}Nd/^{144}Nd vs. ^{147}Sm–^{143}Nd regressions. Thus, just like the variable ^{142}Nd/^{144}Nd ratios reported for other Eoarchean terranes, non-BSE ^{142}Nd/^{144}Nd values of the NSB were inherited from an older component.

1. Introduction

First documented in 2002 (David et al., 2002), the Nuvvuagittuq Supracrustal Belt (hereafter termed NSB) is an arcuate ~8 km^2, dominantly amphibolite supracrustal enclave surrounded by Paleo- to Mesoarchean granitoid gneisses situated at the western edge of the Northeast Superior Province in northern Québec, Canada (Fig. 1). The NSB lies approximately 30 km south of Inukjuak (town), with coastal outcrops close to Porpoise Cove on the eastern shore of Hudson Bay. A minimum age of ca. 3750 Ma for the emplacement of the NSB was previously established from U–Pb zircon geochronology (Cates and Mojzsis, 2007; David et al., 2002, 2009) based on a statistically robust ^{207}Pb/^{206}Pb vs. ^{238}U/^{206}Pb intercept age of 3758^{+51}_{-47} Ma for igneous cores in zircons from trondhjemitic gneisses within the supracrustal succession. Some of these small gneissic bodies locally preserve intrusive contact relationships as revealed by high-resolution (1:50 scale) geologic mapping (Cates and Mojzsis, 2007). Ion microprobe U–Th–Pb depth profiles of two NSB gneiss zircons with concordant igneous cores (3802 ± 12; 3743 ± 26 Ma) yielded age plateaux that reproduce all previously reported igneous and metamorphic ages for the NSB (Cates and Mojzsis, 2009 and references therein). Therefore, these rocks are at least Eoarchean (ca. 3800 Ma) in age and constitute the oldest terrane discovered in the Superior Province. The U–Pb zircon ages reported thus far are broadly similar to the well-known Isua Supracrustal Belt (Nutman et al., 1996) and Akilia association (Manning et al., 2006; Cates and Mojzsis, 2006) outcrops, both of which are part of the upper-amphibolite to granulite metamorphic facies Itsaq Gneiss Complex in southern West Greenland. The NSB is also contemporaneous with emplacement of the oldest parts of the lesser-known Nain Province in Labrador (Nutman and

Abbreviations: MDF, mass-dependent fractionations; MIF, mass-independent fractionations; BSE, Bulk Silicate Earth; NSB, Nuvvuagittuq Supracrustal Belt; IGC, Itsaq Gneiss Complex; SMOW, Standard Mean Ocean Water; CDT, Canyon Diablo Troilite

* Corresponding author at: Department of Geological Sciences, University of Colorado, 2200 Colorado Avenue, UCB 399, Boulder, CO 80309-0399, USA. Tel.: +1 303 492 5014; fax: +1 303 492 2606.
E-mail addresses: mojzsis@colorado.edu, stephen.mojzsis@univ-lyon1.fr (S.J. Mojzsis).

0012-821X/$ - see front matter © 2012 Elsevier B.V. All rights reserved.
http://dx.doi.org/10.1016/j.epsl.2012.11.054

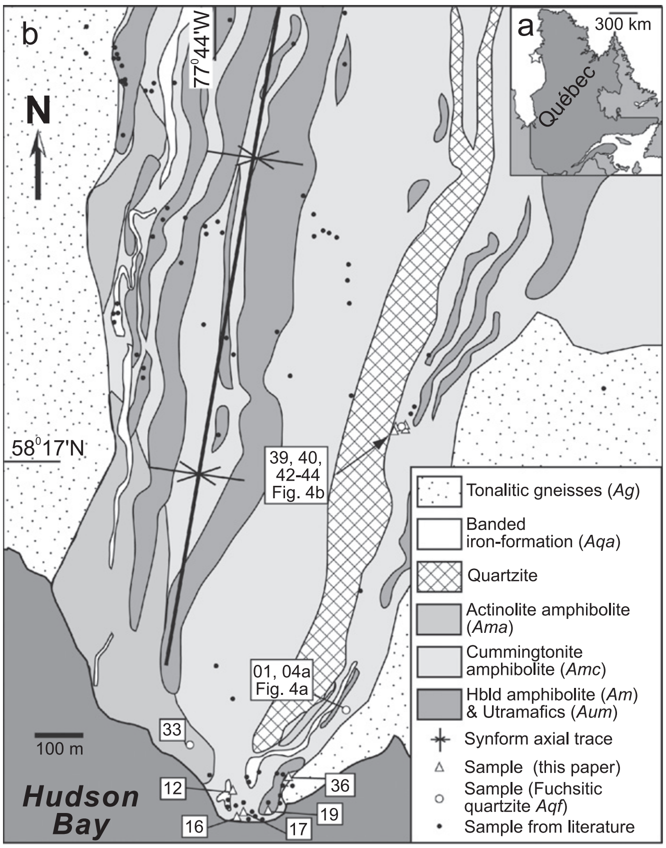

Fig. 1. Geological map and geographic location of the Nuvvuagittuq Supracrustal Belt. (a) Map of Québec with location of NSB indicated and (b) general geologic map of the western limb of the NSB and surrounding tonalitic gneiss with samples indicated (IN080-prefix omitted).
Modified after O'Neil et al. (2007) and David et al. (2009).

Collerson, 1991), and Manfred Complex in Western Australia (Kinny et al., 1988). Like the Itsaq, Nain and Manfred rocks cited above, the NSB hosts quartz–magnetite $\pm$ pyroxene $\pm$ amphibole rocks interpreted as banded iron-formation (BIF; Mloszewska et al., 2012a, 2012b), but unlike those other terranes it preserves common occurrences of quartz–biotite schists (interpreted as "meta-conglomerates" by O'Neil et al. (2007) and Cates and Mojzsis (2007)) with mineralogical and isotopic characteristics consistent with adetrital origin (Dauphas et al., 2007). The discovery of the Nuvvuagittuq Supracrustal Belt is significant not only because of its great antiquity, but also that it is a piece of ancient crust petrogenetically unrelated to the Eoarchean rocks of West Greenland cited above (Cates and Mojzsis, 2007; O'Neil et al., 2007; Roth et al., 2013). The geologic record provided by the NSB adds significantly to a sparsely filled global picture of surface conditions on Earth at about the time life emerged, ostensibly from the ruins of the late heavy bombardment of the solar system approximately 3900 Myr ago (e.g. Abramov and Mojzsis, 2009).

1.1. The problem of placing age constraints on ancient supracrustal belts

Establishing a maximum age for such ancient supracrustal assemblages poses a challenge because the rocks are largely amphibolites ($\pm$ garnet) of basaltic–basaltic andesite composition overprinted by a complex geologic history. Primary igneous zircons, with reliable ages that can be measured by the U–Pb method, are usually rare or absent in such mafic lithotypes so that other less-direct geochronological techniques are required. It was found by O'Neil et al. (2008) that cummingtonite-rich (Ca-poor) amphibolites (as opposed to the usual hornblende-rich amphibolites) in the NSB record deficits in the daughter product (^{142}Nd) of the extinct radionuclide ^{146}Sm, expressed as negative values in the standard μ-notation (e.g. O'Neil et al., 2012). The reported degrees of depletion require that an enriched low Sm/Nd crustal source of these rocks must have been isolated from the ^{142}Nd isotopic evolution of Bulk Silicate Earth (BSE) in the first few hundred million years while ^{146}Sm was still decaying (half-life = 68 $\pm$ 7 Myr; Kinoshita et al., 2012). If it is assumed that the negative μ^{142}Nd anomalies reflect the time these rocks became separated from BSE, regressions through ^{142}Nd/^{144}Nd vs. ^{147}Sm/^{144}Nd space yield a 4362^{+35}_{-54} Ma "scatterchron" (O'Neil et al., 2008, 2012; re-calculated by Roth et al., 2013). If this interpretation is correct, it could make the NSB more than 400 Myr older than the hitherto oldest piece of Earth's crust in the Acasta Gneiss Complex, Northwest Territories of Canada (Bowring et al., 1989). Whole rock ^{147}Sm–^{143}Nd "scatterchron" ages, however, for the same samples are younger: 3891 $\pm$ 584 Ma (Roth et al., 2013). This younger age result agrees well with the previously reported U–Pb zircon geochronology cited above (Cates and Mojzsis, 2007, 2009; David et al., 2009). To resolve this inconsistency in age assignments, and to better interpret the output arising from different radiogenic isotope systems used to explore these rocks, stricter constraints on the formation time of the NSB are required.

1.2. In search of a maximum age for the Nuvvuagittuq Supracrustal Belt

If igneous zircons could be directly found in or associated with any of the cummingtonite-rich amphibolite lithologies that also carry negative μ^{142}Nd, they would allow us to place an upper bounds on the emplacement time(s) of the amphibolites and the associated supracrustal suite. Efforts, however, at obtaining concordant zircons of igneous derivation in the cummingtonite amphibolites have so far been unsuccessful (Sample IN08012; T1 in Supplementary File 2). However, candidate detrital zircons were previously described from some NSB quartz–biotite schists (Cates and Mojzsis, 2007; David et al., 2009). Although these quartz–biotite rocks are a minor lithotype in the NSB, they are nevertheless part of the same supracrustal succession which includes the cummingtonite amphibolite rocks with negative μ^{42}Nd values (O'Neil et al., 2007), and share their deformation history (Nadeau, 2003). Zircons separated from one of these quartz–biotite units have an upper intercept U–Pb regression line age of 3787 $\pm$ 25 Ma (Cates and Mojzsis, 2007), and an oldest individual analysis of 3770 Ma (David et al., 2009). The significance of these ages is that the emplacement of the supracrustals may have been nearly synchronous to the intrusion of the granitoids within the same succession (3758^{+51}_{-47} Ma; Cates and Mojzsis, 2007). Such a temporal relationship has been documented before for detrital sediments (e.g. quartz–biotite schists) captured in Archean supracrustal belts (Nutman et al., 2004).

Field studies were undertaken with the express purpose of searching for more candidate rocks with sedimentary protoliths such as quartzites with typical placer mineral contents (chromite, sulfide, etc.) that also might be expected to contain detrital zircons. Following identification and field mapping (1:5 to 1:50 scale) to guide sampling in the context of the outcrop geology, a variety of geochemical (major-, minor- and trace-elements) and isotopic tools (e.g. U–Pb zircon geochronology, O- and multiple S-isotopes) were applied to (i) establish the origin of these candidate detrital metasedimentary units, and (ii) to address the likelihood that zircons may be contained therein. Zircons were subsequently extracted from these selected samples for textural, U–Pb geochronological, and trace element analysis.

2. Methods

Full sample preparation and analytical techniques used for this study are presented in Supplementary, and a brief description of the protocols is provided here. Homogeneous rock powders were prepared at the University of Colorado in Boulder (CU) following techniques described in Cates and Mojzsis (2006). Whole rock geochemical analyses were performed at the Centre de Recherches Pétrographiques et Géochimiques (CRPG) SARM Facility in Nancy (France) and major, minor and trace element analyses are reported in T1 (Supplementary File 2).

2.1. Whole-rock oxygen isotopes

High-precision oxygen-isotope analyses of sample powder splits were made at the Stable Isotope Laboratory of the Department of Earth and Space Sciences, University of California Los Angeles (UCLA), following the procedures given in Young et al. (1998). Each sample was analyzed multiple times (*n* in T2, Supplementary File 2), and each analysis consisted of 20 cycles of sample-standard comparison. The $\delta^{18}O$ values refer to the per-mil deviation in a sample ($^{18}O/^{16}O$) from SMOW, expressed as $\delta^{18}O=[(^{18}O/^{16}O)_{sample}/(^{18}O/^{16}O)_{SMOW}-1]\times 10^3$. The delta-values were converted to linearized values by calculating: $\delta^{18/17}O'=\ln[(\delta^{18/17}O+10^3)/10^3]\times 10^3$ in order to create straight-line mass-fractionation curves. Results are presented in T2 (Supplementary File 2).

2.2. Multiple sulfur isotopes

Sulfur analyses were made on optically polished petrographic thin sections cast in epoxy with sulfide standards at CU. Following optical mapping and electron microprobe characterization, the thin sections were re-polished and sputter-coated with gold in preparation for ion microprobe analysis following usual procedures (Mojzsis et al., 2003). Multiple sulfur isotopic analyses (^{32}S, ^{33}S, ^{34}S) were made using a Cs^+ microbeam primary ion source and secondary ion beams were focused into adjacent Faraday detectors in multicollection mode on the Cameca ims 1270 ion microprobe at UCLA following the methods as described in Papineau et al. (2007). Data collection, standardization and data reduction procedures follow those presented in Papineau et al. (2005), and reported $\Delta^{33}S$ values (T3, Supplementary File 2) were calculated using the formula $\Delta^{33}S=1000\times[(1+\delta^{33}S/1000)-(1+\delta^{34}S/1000)^{0.518}]$.

2.3. Zircon geochronology and trace elements

All U–Th–Pb geochronology was performed on the UCLA Cameca ims 1270 ion microprobe in monocollection mode. Zircons were handpicked under a binocular microscope from the least magnetic heavy mineral fractions separated using heavy liquids techniques as described in Cates and Mojzsis (2006), then cast in 2.2 cm diameter Buehler© epoxy pucks along with zircon standard AS3 (Black et al., 2003). Zircons were mapped by optical (transmitted and reflected light), back-scattered electrons and/or cathodoluminescence imaging. Geochronological data were collected using standard procedures (e.g. Cates and Mojzsis, 2007) and U–Pb plots were generated using the Isoplot software package (Ludwig, 2001), with results reported in T4 (Supplementary File 2). After the U–Pb analyses were completed, a subset of concordant zircons was selected for further trace element analyses. Rare earth element, and Ti contents translated into Ti-in-zircon thermometry (Ti^{xln}; T5, Supplementary File 2), were collected on the UCLA Cameca ims1270 ion microprobe using the approach described by Schmitt and Vazquez (2006). Analysis spots were ~25 μm in diameter and were positioned to overlap previous geochronology analysis points.

3. Geological and geochemical relations

Major lithologies, metamorphic history and protolith assignments of the NSB have previously been described in Cates and Mojzsis (2007, 2009), O'Neil et al. (2007, 2008, 2011, 2012), David et al. (2009), and Mloszewska et al. (2012a, 2012b). Additional data are provided here which relate to the origins of the "conglomeratic" quartz–biotite schists that host detrital zircon grains, as well as to the ^{142}Nd-anomaly bearing cummingtonite-rich amphibolites. Furthermore, new geochemical and isotopic data are discussed which relate to protolith assignment on previously undescribed chromite-bearing (fuchsitic) quartzites that were found to host detrital zircons. Whole rock geochemical analyses of each of these various units are discussed in context with previously published data and used to assign protolith (Section 5) to facilitate interpretation of the geochronology. A database of compiled geochemical analyses is provided in Supplementary File 3 along with the unit labels used herein; major unit types are also labeled on the map legend in Fig. 1.

3.1. Quartz–biotite schists (Aqbc)

As described in Cates and Mojzsis (2007, 2009), Dauphas et al. (2007), O'Neil et al. (2007, 2011) and David et al. (2009), several centimeter- to meter-thick and laterally continuous quartz–biotite schists (unit label *Aqbc* from Cates and Mojzsis, 2007) occur in the Porpoise Cove area. The rocks contain strongly S-deformed (aspect ratio ~10:1) polymict quartz+gabbro clasts supported in a matrix of biotite with disseminated quartz and minor garnet. They are composed of quartz and biotite, with minor pyrite, magnetite, zircon, chromite and clinozoisite; along with measured Fe-isotopes reported in Dauphas et al. (2007), these compositional characteristics are consistent with a sedimentary origin. In this study, multiple sulfur isotope analyses were made on sulfides from *Aqbc* samples to assess whether they carry mass-independently fractionated (MIF) signatures expected for rocks of marine sedimentary origin in communication with an anoxic Eoarchean atmosphere (Farquhar et al., 2000; Mojzsis et al., 2003). The presence of such MIF signatures would be completely consistent with a sedimentary origin of the *Aqbc* units. Oxygen isotopes were also measured on bulk rock and minerals separates to evaluate this possibility.

3.2. Cummingtonite-rich amphibolites (Amc)

Cummingtonite-rich amphibolites comprise ~70% by visible outcrop area the supracrustal lithologies in the NSB (see Fig. 1). They weather a reddish-brown color, and in freshly broken surfaces otherwise resemble the typical (black) amphibolites of ancient supracrustal belts but for the fact that the dominant amphibole is cummingtonite rather than hornblende. O'Neil et al. (2007, 2008, 2011) have shown that differences between the amphibolite types are reflected in the major element geochemistry, where cummingtonite-rich samples have lower Ca contents at equivalent Mg numbers than the metamorphic equivalents of typical basalts, typical hornblende-containing amphibolites (*Am* and *Amm* unit names of Cates and Mojzsis, 2007). The cummingtonite-rich amphibolites (hereafter: *Amc*) carry the largest reported ^{142}Nd anomalies in the NSB, as opposed to most of the hornblende amphibolites that do not preserve differences resolvable from the terrestrial standard within error (O'Neil et al., 2008; Roth et al., 2013). The *Amc* rocks also have more variable major element concentrations than the hornblende amphibolites. For instance FeO, MnO and Na_2O show a general trend of depletion, and K_2O and P_2O_5 tend to be enriched compared to normal amphibolite. This is also true for SiO_2 which is enhanced in some *Amc* samples (up to 60 wt%) but depleted in others (down to 44 wt%; Cates and Mojzsis, 2007; O'Neil et al., 2007, 2011, Supplementary File 3). Oxygen isotopes were measured on bulk rock and minerals separates of an *Amc* sample to help constrain protolith.

When all available data are compiled together, it is found that *Amc* units can be further divided into three populations based on their Al_2O_3/TiO_2 ratios (e.g. O'Neil et al., 2011): "High" (> 45), "Medium" (26–35) and "Low" (< 25; Fig. 2).

1. Only the "Low" aluminum *Amc* units approach the immobile element (Ti, Al, and V) compositions of hornblende amphibolites from the NSB. Yet, they are enriched in Nb, Zr and Y and depleted in Ni and Cr.
2. As with the *Am* units, the "Low" *Amc* rocks share similarly flat chondrite-normalized REE patterns, and primitive mantle normalized multi-element patterns (Fig. 3).
3. "Medium" *Amc* units are enriched in some immobile elements (Al, Zr, Nb) but depleted in others (Ti, Y, Ni, Cr), and tend to be LREE-enriched; they also have more pronounced negative Nb and Sr anomalies in a multi-element plot compared to "Low" aluminum *Amc* or normal *Am* units (Fig. 3).
4. "High" aluminum *Amc* units are enriched in Al, but depleted in Ti, Zr, Nb, and Y relative to hornblende amphibolites.

The division into three groups based on Al_2O_3/TiO_2 ratios mirrors similar variable aluminum in the ultramafic ("metakomatiite") units that have been mapped in the NSB, where "Barberton-type" (low Al_2O_3/TiO_2), "Munro-type" (medium Al_2O_3/TiO_2), and "High-Al-types" (high Al_2O_3/TiO_2) are all present (O'Neil et al., 2007, 2011). Munro and High-Al ultramafic rock types are depleted in Ti, slightly enriched in Al, enriched in Ni and especially Cr, and depleted in Zr, Nb and Y (High-Al-types more so) relative to Barberton-type.

3.3. *Chromite-bearing quartzites (Aqf)*

Several quartzite bodies occur as cm-scale and laterally continuous (10s m-scale) exposures that share knife-edge contacts and deformation history with cummingtonite-rich amphibolites, hornblende-amphibolites and quartz–biotite conglomerates. No evidence for reaction rims, hydration halos or other features that might be expected for hydrothermal veinings are associated with any of the *Aqf* units identified in this study. Three such outcrops have thus far been found in our field-mapping: one in a glacially polished exposure comprising hornblende- and cummingtonite-amphibolites and quartz–biotite schists (IN08033; F1 in Supplementary File 4); a second unit located just north of the detailed map in Cates and Mojzsis (2007) and directly above a large exposure of quartz–biotite schist (samples IN08001 and IN08004a; Fig. 4a); and a third is intercalated within a thick sequence of cummingtonite-rich amphibolite (IN08039; Fig. 4b).

The *Aqf* rocks are dominated by quartz (70–80%), with about 10% plagioclase, and the remaining mineralogy is composed of phylosillicates (including the Cr-rich muscovite, fuchsite), oxides including chromite, sulfides, and zircons. They are poor in alkalis ($CaO+Na_2O+K_2O<3$ wt%) and have elevated nickel (avg. 63 ppm) and chromium (> 140 ppm) contents (T1 in Supplementary File 2). Rare earth and multi-element plots for the quartzites show strong similarities to previously published patterns for the *Aqbc* units described in Section 3.1 (Fig. 5), and they have sub-chondritic Y/Ho ratios (< 31) that resemble the *Aqbc* units (26–28). Oxygen isotopes bulk rock and mineral separates of two zircon-bearing *Aqf* samples were used to help constrain protolith.

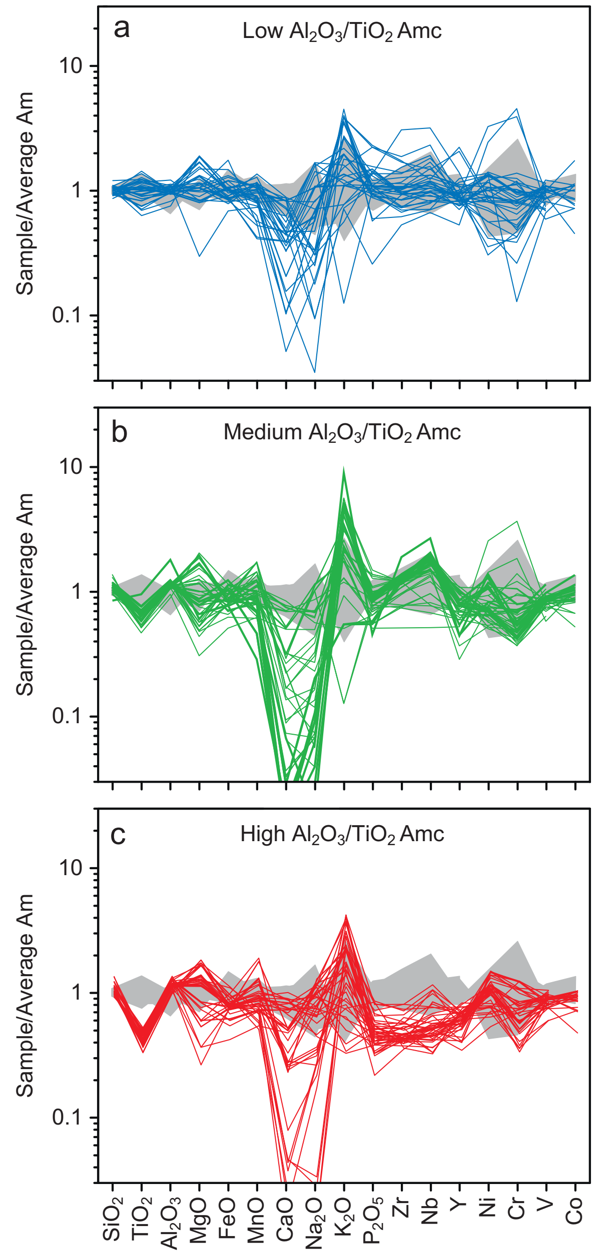

Fig. 2. Major oxide and trace element plots of Low (< 25), Medium (25–35) and High (> 45) Al_2O_3/TiO_2 cummingtonite amphibolites (Amc) normalized to the average hornblende-amphibolite (Am) composition. Gray fields are individual Am compositions normalized to average Am.
Data from O'Neil et al. (2007, 2008, 2011) and Cates and Mojzsis (2007); Supplementary File 3.

4. Results

The principal motivation in this project was to find further lithologies with mineralogical (Section 3) and isotopic ($\delta^{18}O_{VSMOW}$, $\Delta^{33}S$) compositions consistent with a sedimentary origin that could also host detrital zircons. Moreover, it was important that field relations also placed them in close association with cummingtonite-amphibolites previously documented to host ^{142}Nd anomalies. Sample IN08039, a fuchsitic quartzite within an *Amc* outcrop (Fig. 4b) represents one such unit. Other *Aqf* units

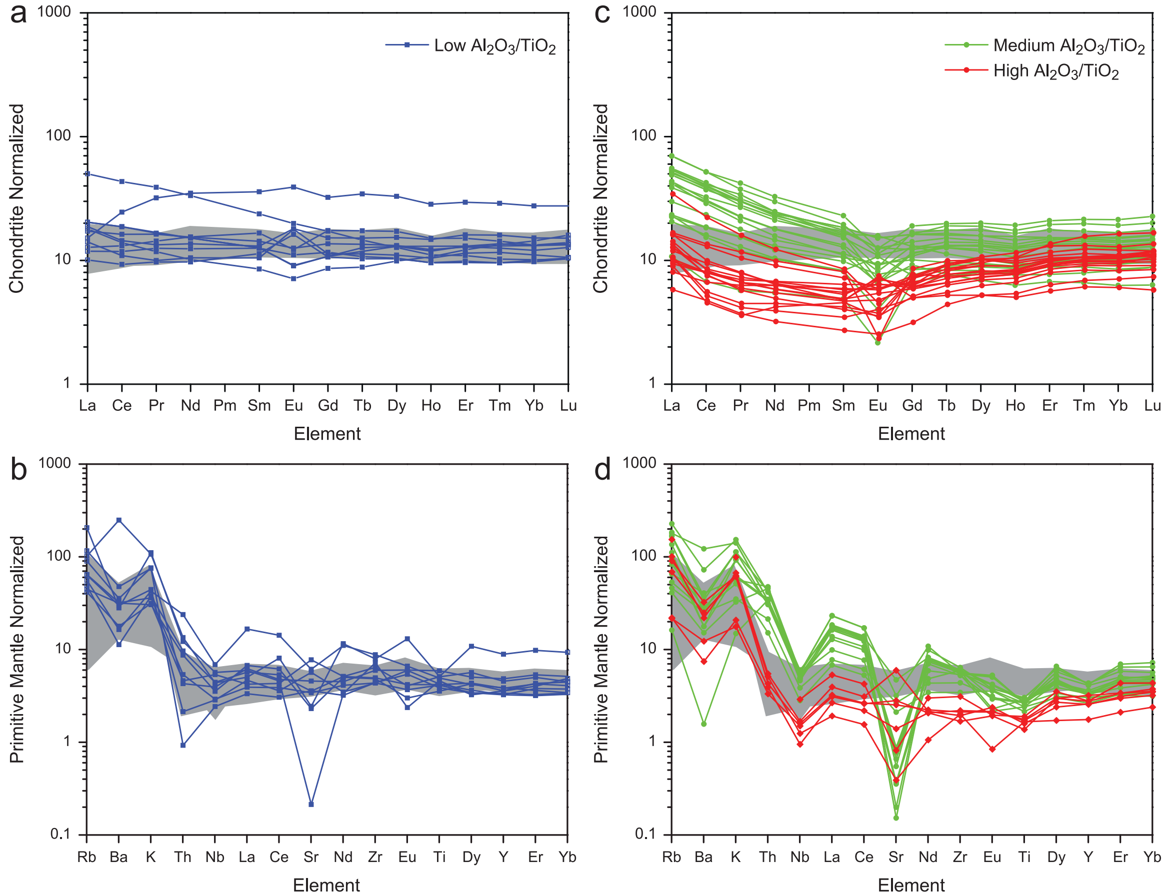

Fig. 3. Multi-element plots of cummingtonite-amphibolites (Amc) as compared to *NSB* hornblende-amphibolites (Am; gray field). (a) Anders and Grevesse (1989) chondrite normalized REE plot for Low Al_2O_3/TiO_2 Amc units. (b) McDonough et al. (1992) Primitive Mantle normalized multi-element plot for Low Al_2O_3/TiO_2 Amc units. (c) Chondrite normalized REE plot for Medium and High Al_2O_3/TiO_2 Amc units. (d) Primitive Mantle normalized multi-element plot for Medium and High Al_2O_3/TiO_2 Amc units. Data from O'Neil et al. (2007, 2008, 2011) and Cates and Mojzsis (2007); Supplementary File 3.

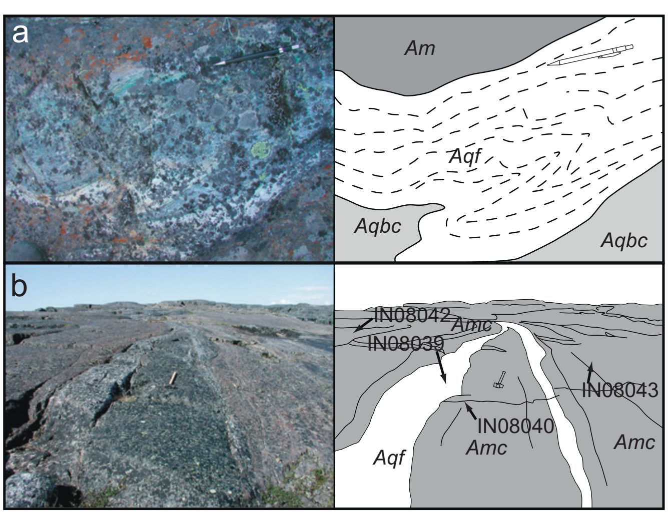

Fig. 4. Field photographs and annotated sketch maps of lithologies discussed in the text. (a) Fuchsitic quartzite (Aqf) adjacent to meta-conglomerate (Aqbc) and hornblende amphibolite (Am); samples IN08001 and IN08004a, taken just to the left of photograph. Pencil for scale. (b) Aqf unit (sample IN08039) folded in cummingtonite amphibolite (Amc; samples IN08040, −042, −043). Hammer is ~1 m long for scale.

were also found closer to the Porpoise Cove outcrops (IN08001, IN08004a, IN08033; Fig. 1) within the same supracrustal succession. Hints that the NSB may have been constructed over a relatively short period of time (< 30 Myr, between 3780 and 3750 Ma) first came to light with the discovery of what were interpreted to be detrital zircons in the quartz–biotite schists (Section 1.2; described in Cates and Mojzsis (2007). The results of zircon geochronology on samples shown to be of sedimentary origin lend support to this hypothesis.

4.1. Whole-rock and mineral O- and multiple S-isotopes

Oxygen isotopes for zircon-bearing fuchsitic quartzites *IN08004a* and *−39* are somewhat enriched in $\delta^{18}O$ (about +10‰; T2 in Supplementary File 2) relative to the gneisses (*IN05003* and *−17*), much like the quartz–biotite schist sample *IN05037*, but less so than the BIFs (*IN08026* and *−32*; +10.71‰ and +11.13‰, respectively). In contrast, the oxygen isotopic composition of cummingtonite-amphibolite samples were found to be somewhat enriched in ^{18}O when compared to typical *Am* units (6.7–8.3‰; T2 in Supplementary File 2). These values are within the range seen in typical Eoarchean amphibolites from Isua (Perry et al., 1978) and Akilia (Manning et al., 2006), and are also similar to values reported for equivalent rocks in the Barberton region in South Africa (Furnes et al., 2007; Hofmann and Harris, 2008). All sulfides measured from the largest, laterally continuous *Aqbc* unit at Porpoise Cove (sample *IN05037* from Cates and Mojzsis, 2007) yield statistically significant positive mass-independent (MIF) $\Delta^{33}S$ anomalies with a weighted mean $\Delta^{33}S$ of $+0.43 \pm 0.07$ (2σ). On the other hand, nearby (< 10 m) hornblende-amphibolites (sample IN05024) have no MIF sulfur (weighted mean $\Delta^{33}S{+}0.03 \pm 0.09$ (2σ); T3 in Supplementary File 2) and lower $\delta^{18}O$ (~+6% to +7‰; T2 in Supplementary File 2).

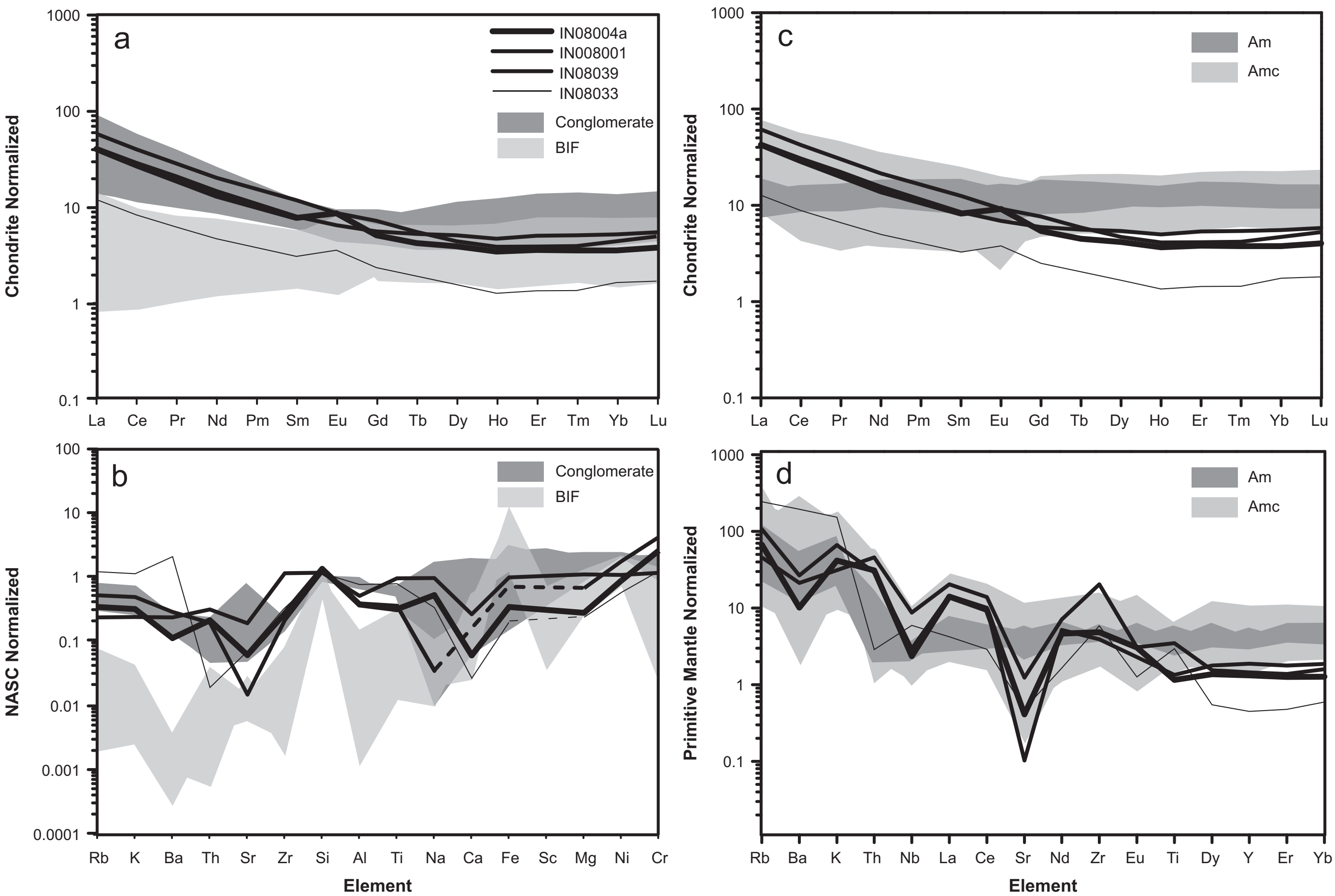

Fig. 5. Multi-element plots of fuchsitic quartzites as compared to NSB BIF, metaconglomerates, hornblende amphibolites (Am) and cummingtonite amphibolites (Amc; gray fields). (a) Anders and Grevesse (1989) chondrite normalized REE plot. (b) Gromet et al. (1984) North American Shale Composite normalized multi-element plot. (c) Anders and Grevesse (1989) chondrite normalized REE plot. (d) McDonough et al. (1992) Primitive Mantle normalized multi-element plot.
Data from O'Neil et al. (2007, 2008, 2011) and Cates and Mojzsis (2007); Supplementary File 3.

4.2. U–Pb geochronology of zircons from fuchsitic quartzites

Abundant zircon yields were obtained from two of the samples (*IN08004a* and *-039*); sample *IN08033* yielded no zircons (F1 in Supplementary File 4). Both zircon-bearing fuchsitic quartzites reported here have distinct age spectra and zircon morphologies consistent with an older detrital component and subsequent overprinting by metamorphic events previously documented for the NSB in Cates and Mojzsis (2009).

4.2.1. Aqf sample IN08004a

A total of 56 analyses on 53 grains yield a cumulative age probability plot with the strongest peak at 3655 Ma, and two smaller peaks at 3722 and 3770 Ma for grains that were less than 10% discordant (Fig. 6). The oldest $^{207}Pb/^{206}Pb$ ages for this sample range from 3718 to 3780 Ma (n=13), and the 7 oldest concordant grains yield a mean age of 3742 ± 48 Ma ((2σ); T4 in Supplementary File 2) that suggests they come from a single source. This conclusion is supported by an MSWD of 1.7 for the *X–Y* ($^{238}U/^{206}Pb$–$^{207}Pb/^{206}Pb$) weighted mean of these analyses, which represents how well the data fit the assumption that the analyses are repeated measurements of the same age (Ludwig, 2001). The calculated concordia age for these data, i.e. the most probable age that the weighed-mean data has on a concordia diagram, is 3742 ± 14 Ma (2σ) with an MSWD = 1.7 (equivalence + concordance). This is an age that is equivalent to, but more precise than, the weighted mean age presented above.

Two types of grain morphologies are present in the oldest zircon population identified in this sample. In addition to the 7 nearly concordant grains, they comprise another 6 grains with (discordant) ages greater than 3720 Ma. Most of the older zircons are slightly rounded with thin overgrowths and strong oscillatory zoning in the cores as seen in back-scattered electron (BSE) images (F4 in Supplementary File 4). Two of the grains are fragments (1_17 and 1_19) that are oriented obliquely such that the internal structure of the zoning is not clear, although both have rims indicating zircon growth at a later time.

These features are markedly different from most of the internal textures of younger ca. 3650 Ma grains, where either sector zoning (e.g. grain 1_9), irregular zoning (e.g. grain 1_3) or weak- to nearly absent zoning (e.g. grain 1_8; F4 and F5 in Supplementary File 4) dominates. Such textures are consistent with metamorphic growth, recrystallization, or the preservation of 'ghost textures' (Hoskin and Schaltegger, 2003). Very nearly all analyses from within this younger group were within about 10% of concordia (18 of 20). This younger population of zircons can be treated statically as a single population, and when this is done, the MSWD of the *X–Y* weighted mean age of 3637 ± 24 Ma (2σ) is 1.3 and the concordia age is 3649 ± 10 Ma (2σ) with an MSWD of 1.4 (concordance + equivalence). This age result is in agreement with, and more precise than, the weighted mean age.

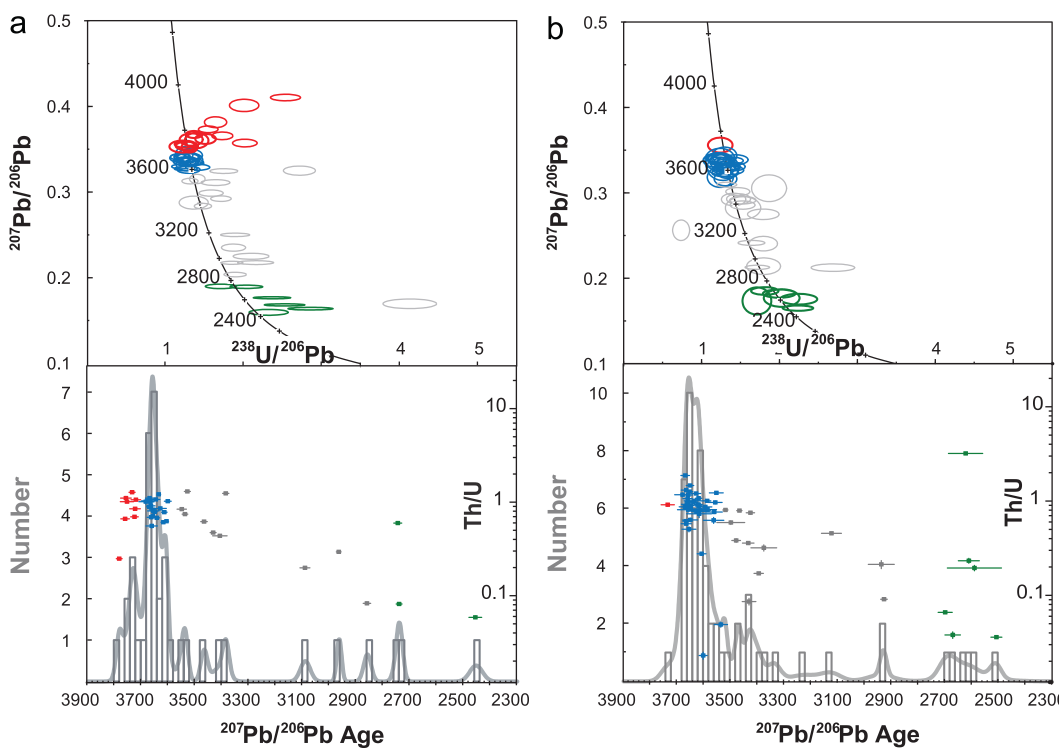

Fig. 6. Integrated geochronology and Th/U geochemistry of zircons from fuchsitic quartzites. Sample localities on Fig. 1. Upper panels are Terra–Wasserberg plots with populations corresponding to separate events (2σ error ellipses). Lower panels are integrated probability and $[Th/U]_{zircon}$ (2σ error bars) for analyses $<10\%$ discordant. (a) IN08004a and (b) IN08039.
Data in T4, Supplementary File 2.

The youngest zircons analyzed here are typified by "spongy" internal structures often described for hydrothermal growth (Hoskin and Schaltegger, 2003). Zircon Th/U values ($[Th/U]_{zirc}$) of the different age populations are in accordance either with equilibrium growth in a granitic melt or various modes of metamorphic, solid-state and/or hydrothermal growth (Hoskin and Black, 2000; T4 in Supplementary File 2). The $[Th/U]_{zirc}$ of the oldest zircons are consistent with equilibrium growth in a rock with the composition of a granite-granitoid (predicted $[Th/U]_{zirc}=$ 0.6–1.0, based on a $\sim$0.2 rock/zircon fractionation; Mahood and Hildreth, 1983; Mojzsis and Harrison, 2002).

4.2.2. *Aqf sample IN08039*

Our 65 analyses on 65 grains yield a cumulative probability plot with a strong age peak at 3650 Ma calculated from 50 analyses that are $<10\%$ discordant (Fig. 6). A single concordant analysis of 3733 ± 50 Ma (2σ) represents a reliable age assignment for this older component. This age comes from a core region with faint oscillatory zoning in a rounded and broken zircon that has a thick rim overgrowth in BSE (grain 2_2; F4 in Supplementary File 4). Grains from the ca. 3650 Ma group have a variety of morphologies, but tend to be irregularly shaped with sector zoning (F5 in Supplementary File 4). This suggests that they, like the ca. 3650 Ma zircons in sample IN08004a, are of metamorphic origin. If the analyses that fall under this peak are treated as a single population, they yield a weighted mean age of 3632 ± 18 Ma (2σ), with an MSWD of the *X–Y* weighted mean of 1.6. The concordia age is equivalent at 3634 ± 24 Ma (2σ) with an MSWD of 1.6 (concordance+equivalence). The internal morphologies of youngest zircons from this sample are also similar to those from the ca. 3650 Ma population, but are more inclusion rich.

4.2.3. *Zircon trace element analyses*

Zircon REE analysis reveals that concentrations in the metamorphic grains (all crystals with ages younger than ca. 3650 Ma) are enriched in the MREE and HREE and have subdued Ce* anomalies relative to the oldest age population. The oldest zircons in our sample suite (ca. 3780 Ma) have similar chondrite-normalized REE patterns distinct from slightly younger (3718–3732 Ma) populations. These somewhat younger zircons have strongly depleted LREE values, and are more enriched in MREE and HREE (Fig. 7, T5 in Supplementary File 2) relative to the oldest zircons. The REE patterns for this slightly younger population are also indistinguishable from the ca. 3627–3675 Ma metamorphic group. A similar pattern of REE depletions has been observed in metamorphic rims vs. cores of zircons from the contemporaneous Itsaq gneisses in West Greenland (Whitehouse and Platt, 2003). The oldest zircon cores have igneous-type REE patterns completely consistent to those previously reported for igneous zircons from intrusive NSB trondhjemitic gneisses (Cates and Mojzsis, 2009), with only a slight relative enrichment in the MREE (Nd–Gd).

5. Protolith assignments

It is important to note that large kilometer-sized enclaves of ancient mostly (mafic) amphibolite rocks – locked in highly deformed granitoid gneiss complexes – are more accurately described by the geologic term "Supracrustal Belt" rather than the generic "Greenstone Belt". That is because the field term "greenstone" connotes a specific petrogenetic meaning for low-grade metamorphic assemblages of (green) chlorite, epidote and actinolite. However, "greenstone" assemblages are only a minor retrogressed component of the NSB (Mloszewska et al., 2012a, 2012b; O'Neil et al., 2012) compared to the dominantly (black)

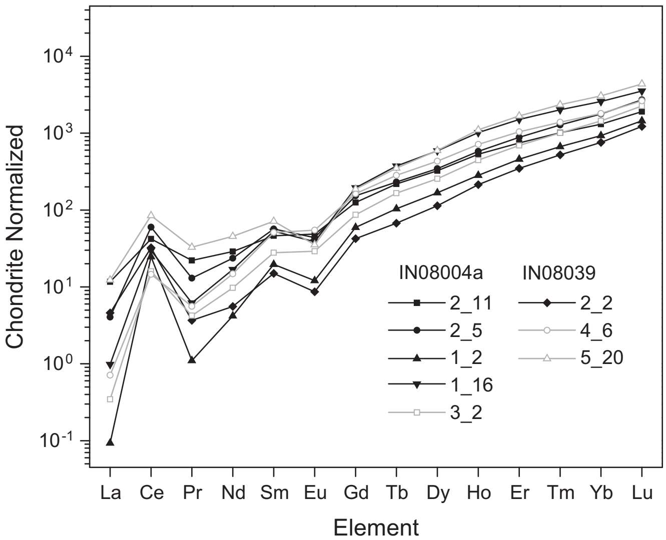

Fig. 7. Anders and Grevesse (1989) chondrite normalized REE analyses of individual zircons. Black filled symbols are from the ca. 3740 Ma population and gray open symbols are from the ca. 3650 Ma population.
Data in T5, Supplementary File 2.

upper amphibolite-facies rocks that comprise ~70% of outcrop (Cates and Mojzsis, 2009). Hence, the name Nuvvuagittuq Supracrustal Belt is a more accurate reflection of the metamorphic history of the NSB (cf. O'Neil et al., 2007), just as it is used for the contemporaneous enclaves of the Eoarchean (3770–3810 Ma) Isua Supracrustal Belt in southern West Greenland (Nutman et al., 1996). Given this metamorphic history, identification of protoliths in ancient supracrustal terranes is a challenge: primary sedimentary or igneous features and minerals are altered or destroyed; elements are mobilized; deformation can obscure or destroy original contact relationships, and radiogenic isotopic signatures can be re-set in all but the most robust systems.

5.1. Quartz–biotite schists

Published interpretations of the quartz–biotite schists agree that they are most likely detrital sediments (Cates and Mojzsis, 2007; David et al., 2009), but alternate hypotheses for their origin must be explored. They may be highly deformed and boudinaged chemical sediments or boudinaged quartz veins, and both BIF and cummingtonite-amphibolites with extensive quartz veining occur in the NSB. Previous geochemical studies highlighted the similarities these rocks have to Archean shales in trace element composition, elevated Ni and Cr contents, and sub-chondritic Y/Ho (Cates and Mojzsis, 2007). This interpretation is now bolstered by new oxygen isotope data and the multiple sulfur isotope compositions of disseminated pyrite (Section 4.1). All pyrite grains within an *Aqbc* schist sample were shown to carry mass-independently fractionated (MIF) sulfur isotopes, and an immediately adjacent amphibolite (*IN05024*) yielded values indistinguishable from the terrestrial mass-dependent fractionation line with not a single analysis deviating (within error) from mass dependence (Fig. 8; T3 in Supplementary File 2). This particular result shows that at least for the NSB Porpoise Cove outcrops, MIF sulfur transport from neighboring rocks at some later date was an unimportant process. The only other lithology thus far documented with MIF sulfur isotopes in the NSB is a quartz–magnetite rock (BIF; sample *IN05007*) with a weighted mean Δ^{33}S of $+0.68 \pm 0.13$.

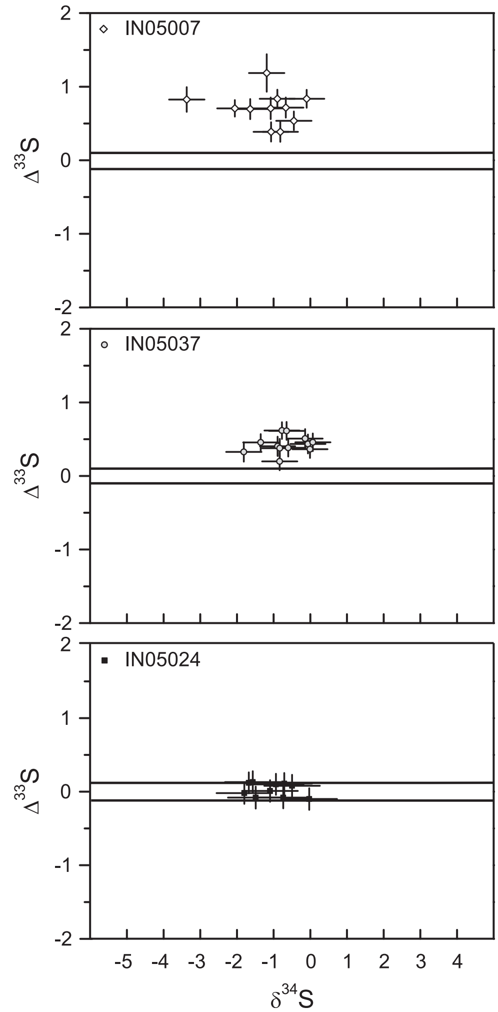

Fig. 8. δ^{24}S vs. Δ^{33}S plots with mass-dependent band (0.0 ± 0.3) indicated. Error bars are 1σ external error: (a) BIF sample, (b) Quartz–biotite schist (metaconglomerate) sample and (c) Hornblende amphibolite sample.
Data in T3, Supplementary File 2.

5.2. Cummingtonite-amphibolites

Despite superficial similarities, an examination of geochemical data for the *Amc* rocks – including those known to host anomalous μ^{142}Nd – indicates that cummingtonite-rich amphibolites are unlikely to simply be the in situ weathering product of the precursor basalts of the hornblende amphibolites. Only the "Low" aluminum *Amc* units (Section 3.2) come close to matching compositions with hornblende-rich amphibolites via similarly flat chondrite-normalized REE patterns and primitive mantle normalized multi-element plots. However, if the low Al_2O_3/TiO_2 amphibolite units are co-genetic to the hornblende amphibolites, the expectation is that they should also share proportions of other immobile elements; isocon analysis of the relative proportions of these elements could provide clues to possible alteration processes (Grant, 2005; Fig. 9, T6 in Supplementary File 2).

The slope of the isocon in Fig. 9 is ~1, which means that there was no wholesale gain or loss of mass or volume if the Low-Al_2O_3/TiO_2 *Am* and *Amc* units were cogenetic. The Low-Al_2O_3/TiO_2 cummingtonite-rich rocks are invariably enriched in the immobile elements Zr (9–40%) and Nb (8–45%) and depleted in Cr (12–38%), with smaller variations in Y and Ni when compared to the hornblende-amphibolites. They are enriched in the mobile oxides and elements such as MgO (20–30%), K_2O (70–130%); P_2O_5

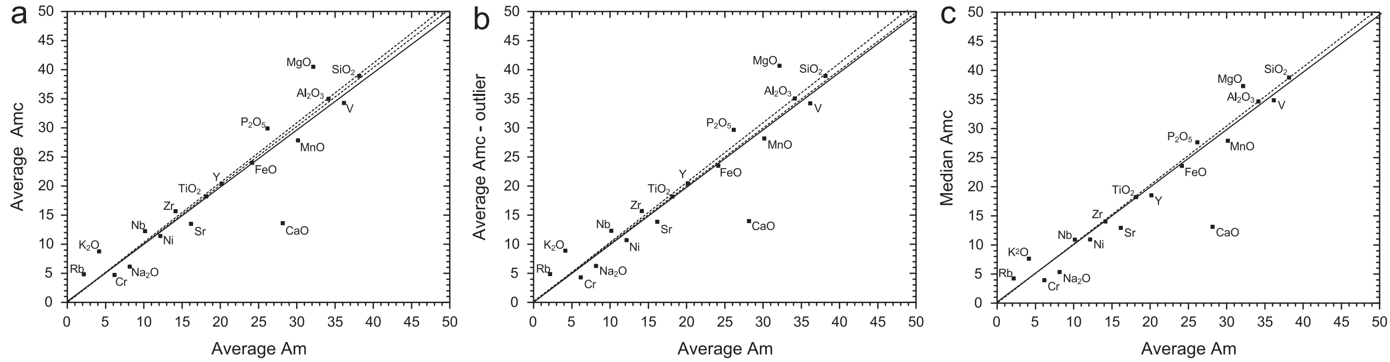

Fig. 9. Isocon diagrams for amphibolites comparing average hornblende-amphibolites (Am) to cummingtonite-amphibolites (Amc). (a) Unfiltered Low Al_2O_3/TiO_2 Amc average; (b) low Al_2O_3/TiO_2 Amc average excluding sample PC-176 which has extraordinarily high Cr and Ni counts ($\sim 10\times$ other Amc units); (c) median of Low Al_2O_3/TiO_2 Amc. Solid line is isocon calculated from linear fit of SiO_2, Al_2O_3, TiO_2, FeO and V through the origin. Dashed lines are isocons assuming that either TiO_2 or Al_2O_3 were immobile. Data from O'Neil et al. (2007, 2008) and Cates and Mojzsis (2007); Supplementary data File 3.

(35–40%) and Rb (90–155%), while depleted in MnO (10–15%), Na_2O ($\sim$30%), CaO (55–60%), and Sr (25–35%). In principle, these variations are consistent with an immature sedimentary protolith, where variations Zr and Cr abundances would be controlled by variable chromite and zircon contents during deposition. This interpretation is supported by a wide range of, but increasingly depleted trend in Ca and Na as seen in traditional weathering plots (F2 in Supplementary File 4). Owing to the fact that these plots do not incorporate MgO, they cannot distinguish between weathering and some types of alteration. Hence, alone they are not a definitive indication of a sedimentary origin. Thus, other possibilities to explain their composition, such as silicification, metasomatism or hydrothermal alteration must be considered.

Despite evidence of widespread silicification in other Archean volcano-sedimentary sequences such as the Barberton and Pilbara greenstone belts (de Vries et al., 2004; Hofmann and Harris, 2008; Rouchon and Orberger, 2008; Van Kranendonk et al., 2002), there is little indication that the *Amc* rocks became CaO-poor via this process. Only 3 of 12 samples examined here have more than $\sim$10% enrichment in SiO_2 compared to typical hornblende amphibolite. There is no evidence for a volume increase (isocon slope ≈ 1 in Fig. 9), and while there are depletions in CaO, MnO and Na_2O, the expected corresponding depletion in MgO is absent. Similarly, evidence is lacking for potassic metasomatism beyond some elevated K_2O and Rb values compared to hornblende amphibolite. During K-metasomatism MgO and FeO should be removed almost as efficiently as CaO (Hanor and Duchac, 1990). Both Nb and Zr should be immobile in most circumstances, but consistent enrichments in these elements vs. the hornblende amphibolites point to a different history for the "Low" Al_2O_3/TiO_2 *Amc* units.

Based on major element enrichments and depletions, and the relatively good correlation between immobile trace elements, an origin for the cummingtonite amphibolites as highly weathered and/or pyroclastic deposit was previously proposed (O'Neil et al., 2011). Precedents exist for rocks of this composition: low CaO contents could have arisen from hydrothermal alteration of the chemical composition of matrix plagioclase in pyroclastic deposits via seawater (NaCl) brines at high temperatures (>500 °C). This action albitizes the plagioclase releasing Ca as $CaCl_2$ and $Ca(OH)_2$ for example in the reaction: clinopyroxene + calcic plagioclase + NaCl-fluid $\rightarrow$ amphibole + sodic plagioclase (e.g. Harigane et al., 2011; Spear, 1981). It is noteworthy that cummingtonite $(Mg,Fe^{2+})_2(Mg,Fe^{2+})_5[Si_8O_{22}](OH)_2$ is polymorphic with anthophyllite $(Mg,Fe^{2+})_7[Si_8O_{22}](OH,F)_2$. A comparable rock to the NSB cummingtonite amphibolite in both age and composition was described in the Akilia association by Manning et al. (2006) as an "anthophyllite-garnet" rock of probable volcano-clastic sedimentary origin. The *Amc* rocks probably started off as mafic/ultramafic tuffs that experienced high-temperature seawater NaCl–brine albitization.

5.3. Fuchsitic quartzites

Silicification and K-metasomatism are common features of Archean sequences as a result, for example, of flow-top alteration caused by hydrothermal alteration (e.g. Hofmann and Harris, 2008). It makes sense to test whether the sampled *Aqf* units are not detrital in origin, but are instead silicified flow-tops, quartz veins, or highly altered/deformed banded-iron or banded-silicate formation (e.g. Mloszewska et al., 2012a, 2012b).

The most obvious candidate for a silicified end-member is sample *IN08039*, a quartzite within a thick sequence of "Low" Al_2O_3/TiO_2 cummingtonite amphibolites (Section 4.2.2). Several duplicate samples of *Amc* from this locality have had geochemical analyses performed: IN08040, −43, 44 and samples PC-171, −173A and −173B of O'Neil et al. (2007) (T1 in Supplementary File 2; Supplementary File 3). Attempts at detecting silicification with isocon diagrams with sample IN08039 as the "most altered", and any of the nearby *Amc* samples as the "least altered", yielded poor results. Quartzite *IN08039* is enriched in the immobile elements Zr and Nb as well as TiO_2, relative to Al_2O_3, and depleted in Y and V (F2 in Supplementary File 4). Overall, *Aqf* lithologies in the NSB are enriched in LREEs and depleted in HREEs when compared to both hornblende- and cummingtonite-amphibolites, and they tend to have negative Nb anomalies on a multi-element plot (Fig. 5d). This is unlike what is seen in silicified mafic rocks, where all the REE concentrations become depleted with increased silicification, and there is no change in degree of Nb, or Ti anomalies (Hofmann and Harris, 2008).

Trace element analyses also show that the quartzites did not originate as quartz veins. In the Barberton Greenstone Belt, both chert veins and bedded cherts are mostly an order of magnitude more depleted in REEs, Y, Nb, Zr, Ni and Cr than the associated hydrothermally altered basalts and komatiites (e.g. Hanor and Duchac, 1990). Similar patterns are also seen in quartz veinings in younger rocks, including those in granitoid systems (Neiva et al., 1990) and metapelitic schists (Janots et al., 2006). Oxygen isotopic values ($\delta^{18}O_{VSMOW}$) of around +10‰ (T2 in Supplementary File 2) are different from neighboring hornblende- and cummingtonite-amphibolites ($\delta^{18}O$ ranges from +6.2% to +8.8‰) but consonant with a sedimentary source, again like the quartz–biotite schists.

The *Aqf* rocks are poor in alkalis ($CaO+Na_2O+K_2O<3$ wt%) and yet they have elevated Ni (>50 ppm) and Cr (>140 ppm) contents (T1 in Supplementary File 2). This composition excludes the possibility that they are altered granitoid (tonalite or trondhjemite) gneisses, which are relatively depleted in Cr by a factor of

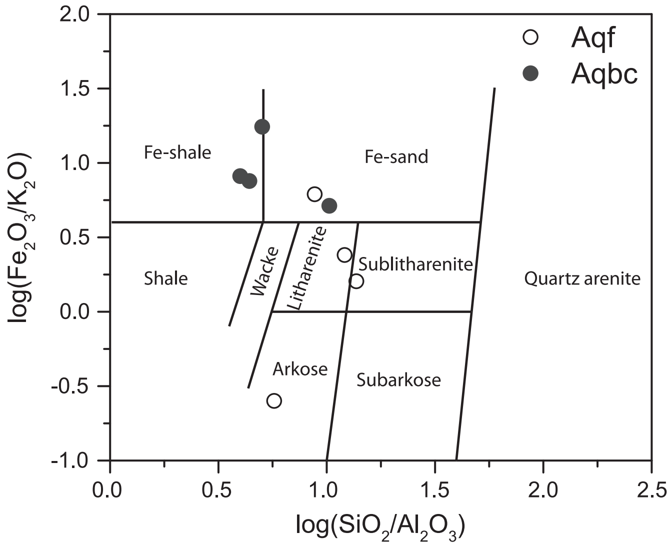

Fig. 10. Classification diagram for terrigenous sandstones and shales using log(Fe_2O_3/K_2O) vs. log(SiO_2/Al_2O_3) of Herron (1988). Quartz–biotite schists (Aqbc) and fuchsitic quartzites (Aqf) plotted. Chemical sediments plot outside the fields of the diagram.

2 and in Ni by an order of magnitude (Cates and Mojzsis, 2007). In multi-element and REE plots, the *Aqf* units most resemble previously published data for the quartz–biotite (*Aqbc*) schists and are distinct from BIF and amphibolite patterns (Fig. 5b and d). The *Aqf* rocks do not have elevated Y/Ho ratios typical of chemical sediments such as BIF (<31; e.g. Bolhar et al., 2005) but are indistinguishable from the quartz–biotite units.

All indications are that the *Aqf* units originated as quartz sands with a heavy mineral suite dominated by zircon, sulfide and chromite. When plotted on the sedimentary discrimination diagram of Herron (1988), they sit within the fields of arkose to litharenite, whereas the quartz–biotite schists plot in the less mature fields of Fe-sand to Fe-shale, and chemical sediments do not plot within Herron's field boundaries at all (log(Fe_2O_3/K_2O) >3; Fig. 10). They are not mechanically or compositionally modified chemical sediments, nor are they quartz veins, altered granitoid gneisses or silicified cummingtonite amphibolites.

6. Conclusions

The results of analyses on detrital zircon ages of igneous derivation in quartzites and quartz–biotite schists of the Nuvvuagittuq Supracrustal Belt show that these rocks – including the cummingtonite-amphibolites that preserve low $^{142}Nd/^{144}Nd$ reported in O'Neil et al. (2008, 2012) and Roth et al. (2013) – do not represent relict Hadean mafic crust that formed at ca. 4400 Ma (O'Neil et al., 2012).

Comparisons of zircon ages from multiple lithologies in the NSB show that its initial development took place around 3800 Ma over a span of less than 30 Myr prior to a protracted metamorphic history. This conclusion is based on the age of the oldest near concordant (92%) detrital zircon at 3780 ± 22 Ma (2σ) and the established age of intrusive trondhjemitic gneisses at 3758^{+51}_{-47} Ma (Cates and Mojzsis, 2007). Many zircons were then reset or grew during a metamorphic event at ca. 3650 Ma (possibly earlier; Section 4.2.1). This age agrees well with documented ages for overgrowths on igneous zircons at 3622 ± 47 Ma reported in Cates and Mojzsis (2009). It also matches the igneous emplacement time for a suite of tonalitic gneissesin the central part of the NSB (3661 ± 4 Ma; David et al., 2009; Fig. 1).

The absence of concordant pre-3800 Ma zircons in any NSB lithotype thus far analyzed opens the possibility that the cummingtonite amphibolites could have been derived in part from reworked juvenile non-zircon-bearing crustal components. As such, variable and imprecise Nd model ages of 4100–4400 Myr (David et al., 2009; O'Neil et al., 2007, 2008, 2012) might represent an average sedimentary provenance age (e.g. Yamashita et al., 2000). Otherwise, if NSB cummingtonite amphibolite protolith was an altered volcanic rock, the negative μ^{142}Nd values became assimilated from recycling of an older crustal component or enriched mantle source (Roth et al., 2013; Guitreau et al., 2013). Our results are in line with the notion that the last vestiges of primordial crust that held a geochemical memory of very early (pre-4500 Ma) silicate differentiation, was destroyed in the Archean in what was the culmination of more than a half-billion years of crustal evolution that began in the early Hadean.

Acknowledgments

We have benefitted from discussions and debates with F. Albarède, W. Bleeker, J. Blichert-Toft, B. Bourdon, R. Carlson, D. Francis, M. Guitreau, K. Konhauser, A. Mloszewska, J. O'Neil, A. Roth, R. Stevenson and E. Thomassot. The manuscript was improved thanks to thorough and constructive reviews by B. Kamber and an anonymous reviewer, and editorial handling by T. Elliot. Logistical assistance for work in the Nuvvuagittuq Supracrustal Belt from the Pituvik Corporation of Nunavik (Québec) is gratefully acknowledged. NLC and SJM acknowledge support from the NASA Exobiology and Evolutionary Biology Program. Additional support to SJM came from the National Geographic Society, University of Colorado, and the J. William Fulbright Foundation. KZ is grateful for support from the NASA Astrobiology Institute. AKS acknowledges facility support to the UCLA ion microprobe center from the Instrumentation and Facilities Program of the US National Science Foundation.

Appendix A. Supporting information

Supplementary data associated with this article can be found in the online version at http://dx.doi.org/10.1016/j.epsl.2012.11.054.

References

Abramov, O., Mojzsis, S.J., 2009. Microbial habitability of the terrestrial biosphere during the late heavy bombardment. Nature 459, 419–422.
Anders, E., Grevesse, N., 1989. Abundances of the elements—meteoric and solar. Geochim. Cosmochim. Acta 53 (1), 197–214.
Black, L.P., Kamo, S.L., Williams, I.S., Mundil, R., Davis, D.W., Korsch, R.J., Foudoulis, C., 2003. The application of SHRIMP to Phanerozoic geochronology; a critical appraisal of four zircon standards. Chem. Geol. 200, 171–188.
Bolhar, R., Kamber, B.S., Moorbath, S., Whitehouse, M.J., Collerson, K.D., 2005. Chemical characterization of earth's most ancient clastic metasediments from the Isua Greenstone Belt, southern West Greenland. Geochim. Cosmochim. Acta 69, 1555–1573.
Bowring, S.A., Williams, I.S., Compston, W., 1989. 3.96 Ga gneisses from the Slave province, Northwest Territories, Canada. Geology 17, 971–975.
Cates, N.L., Mojzsis, S.J., 2009. Metamorphic zircon, trace elements and Neoarchean metamorphism in the ca. 3.75 Ga Nuvvuagittuq supracrustal belt, Quebec (Canada). Chem. Geol. 261, 98–113.
Cates, N.L., Mojzsis, S.J., 2006. Chemical and isotopic evidence for widespread Eoarchean metasedimentary enclaves in southern West Greenland. Geochim. Cosmochim. Acta 70, 4229–4257.
Cates, N.L., Mojzsis, S.J., 2007. Pre-3750 Ma supracrustal rocks from the Nuvvuagittuq supracrustal belt, northern Quebec. Earth Planet. Sci. Lett. 255, 9–21.
Dauphas, N., Cates, N.L., Mojzsis, S.J., Busigny, V., 2007. Identification of chemical sedimentary protoliths using iron isotopes in the >3760 Ma Nuvvuagittuq supracrustal belt, Canada. Earth Planet. Sci. Lett. 254, 358–376.
David, J., Stevenson, R.K., Nadeau, P., Godin, L., 2002. La séquence supracrustale de Porpoise Cove, région d'Inukjuak: un exemple unique de croûte paléo-archéenne

(ca. 3.8 Ga) dans la Province du Supérieur. In: L'exploration minérale au Québec, notre savoir, vos découvertes. Ministère des Ressources Naturelles, Québec. DV 2002, pp. 17.
David, J., Godin, L., Stevenson, R.K., O'Neil, J., Francis, D., 2009. U–Pb ages (3.8–2.7 Ga) and Nd isotope data from the newly identified Eoarchean Nuvvuagittuq supracrustal belt, Superior Craton, Canada. Geol. Soc. Am. Bull. 121, 150–163.
de Vries, S.T., Pryer, L.L., Fry, N., 2004. Evolution of Neoarchaean and Proterozoic basins of Australia. Precambrian Res. 166, 39–53.
Farquhar, J., Bao, H., Thiemens, M., 2000. Atmospheric influence of Earth's earliest sulfur cycle. Science 289, 756–758.
Furnes, H., de Wit, M., Staudigel, H., Rosing, M., Muehlenbachs, K., 2007. A vestige of Earth's oldest ophiolite. Science 315, 1704–1707.
Grant, J.A., 2005. Isocon analysis: a brief review of the method and applications. Phys. Chem. Earth 30, 997–1004.
Gromet, L.P., Haskin, L.A., Korotev, R.L., Dymek, R.F., 1984. The "North American shale composite": its compilation, major and trace element characteristics. Geochim. Cosmochim. Acta 48, 2469–2482.
Guitreau, M., Blichert-Toft, J., Mojzsis, S.J., Roth, A.S.G., Bourdon, B., 2013. A legacy of Hadean silicate differentiation inferred from Hf isotopes in Eoarchean rocks of the Nuvvuagittuqsupracrustal belt (Québec, Canada). Earth Planet. Sci. Lett. 362, 171–181.
Hanor, J.S., Duchac, K.C., 1990. Isovolumetric silicification of early Archean komatiites: geochemical mass balances and constraints on origin. J. Geol. 98, 863–877.
Harigane, Y., Michibayashi, K., Ohara, Y., 2011. Deformation and hydrothermal metamorphism of gabbroic rocks within the Godzilla Megamullion, Parece Vela Basin, Philippine Sea. Lithos 124, 185–199.
Harrison, T.M., 2009. The Hadean crust: evidence from >4 Ga zircons. Annu. Rev. Earth Planet. Sci. 37, 479–505.
Herron, M., 1988. Geochemical classification of terrigenous sands and shales from core or log data. J. Sed. Pet. 58, 820–829.
Hofmann, A., Harris, C., 2008. Silica alteration zones in the Barberton greenstone belt: a window into subseafloor processes 3.5–3.3 Ga ago. Chem. Geol. 257, 221–239.
Hoskin, P.W.O., Schaltegger, U., 2003. The composition of zircon and igneous and metamorphic petrogenesis. Rev. Min. Geochem. 53, 27–62.
Hoskin, P.W.O., Black, L.P., 2000. Metamorphic zircon formation by solid-state recrystallization of protolith igneous zircon. J. Met. Geol. 18, 423–439.
Janots, E., Negro, F., Brunet, F., Goffé, F., Engi, B., Bouybaouène, M.L., M., 2006. Evolution of the REE mineralogy in HP–LT metapelites of the Sebtide complex, Rif, Morocco: monazite stability and geochronology. Lithos 87, 214–234.
Kinny, P.D., Williams, I.S., Froude, D.O., Ireland, T.R., Compston, W., 1988. Early Archaean zircon ages from orthogneisses and anorthosites at Mount Narryer, Western Australia. Precambrian Res. 38, 325–341.
Kinoshita, N., Kashiv, M., Collon, Y., Deibel, P., DiGiovine, C.M., Greene, B., Henderson, J.P., Jiang, D.J., Marley, C.L., Nakanishi, S.T., Pardo, T., Rehm, R.C., Robertson, K.E., Scott, D., Schmitt, R., Tang, C., Vondrasek, X.D., Yokoyama, R., 2012. A shorter ^{146}Sm half-life measured and implications for ^{146}Sm–^{142}Nd chronology in the solar system. Science 335, 1614–1617.
Ludwig, K.R., 2001. User's Manual for Isoplot/Ex Rev. 2.49: A Geochronological Toolkit For Microsoft Excel. Berkeley Geochronological Center Special Publication 1a.
Mahood, G., Hildreth, W., 1983. Large partition coefficients for trace elements in high-silica rhyolites. Geochim. Cosmochim. Acta 47, 11–30.
Manning, C.E., Mojzsis, S.J., Harrison, T.M., 2006. Geology, age and origin of supracrustal rocks, Akilia, west Greenland. Am. J. Sci. 306, 303–366.
McDonough, W.F., Sun, S.-S., Ringwood, A.E., Jagoutz, E., Hofmann, A.W., 1992. Potassium, rubidium, and cesium in the Earth and Moon and the evolution of the mantle of the Earth. Geochim. Cosmochim. Acta 56, 1001–1012.
Mloszewska, A.M., Pecoits, E., Cates, N.L., Mojzsis, S.J., O'Neil, J., Robbins, L.J., Konhauser, K.O., 2012a. The composition of Earth's oldest iron-formations: the Nuvvuagittuq supracrustal belt (Quebec, Canada). Earth Planet. Sci. Lett. 317, 331–342.
Mloszewska, A.M., Mojzsis, S.J., Pecoits, E., Papineau, D., Dauphas, N., Konhauser, K.O., 2012b. Chemical sedimentary protoliths of the >3.75 Ga Nuvvuagittuq Supracrustal Belt (Québec, Canada). Gondwana Res 23, 574–594.
Mojzsis, S.J., Harrison, T.M., 2002. Establishment of a 3.83-Ga magmatic age for the Akilia tonalite (southern West Greenland). Earth Planet. Sci. Lett. 202, 563–576.
Mojzsis, S.J., Coath, C.D., Greenwood, J.P., McKeegan, K.D., Harrison, T.M., 2003. Confirmation of mass-independent isotope effects in Archean (2.5–3.8 Ga) sedimentary sulfides as determined by ion microprobe analysis. Geochim. Cosmochim. Acta 67, 1635–1658.
Nadeau, P., 2003. Structural Investigation of the Porpoise Cove Area, Northeast Superior Province, Northern Québec. Unpublished M.Sc. Thesis. Simon Fraser University.
Neiva, A.M.R., Neiva, J.M.C., Silva, M.M.V.G., 1990. Geochemistry of gold quartz vein walls from Jales (northern Portugal). Chem. Geol. 82, 217–251.
Nutman, A.P., Collerson, K.D., 1991. Very early Archean crustal–accretion complexes preserved in the North Atlantic craton. Geology 19, 791–794.
Nutman, A.P., Friend, C.R.L., Barker, S.L.L., McGregor, V.R., 2004. Inventory and assessment of Paleoarchaean gneiss terrains and detrital zircons in southern West Greenland. Precambrian Res. 135, 281–314.
Nutman, A.P., McGregor, V.R., Friend, C.R.L., Bennett, V.C., Kinny, P.D., 1996. The Itsaq Gneiss Complex of southern West Greenland; the world's most extensive record of early crustal evolution (2900–2600 Ma). Precambrian Res. 78, 1–39.
O'Neil, J., Carlson, R.W., Paquette, J.-L., Francis, D., 2012. Formation age and metamorphic history of the Nuvvuagittuq Greenstone Belt. Precambrian Res. 220–221, 23–44.
O'Neil, J., Francis, D., Carlson, R.W., 2011. Implications of the Nuvvuagittuq greenstone for the formation of Earth's early crust. J. Petrol. 52, 985–1009.
O'Neil, J., Carlson, R.W., Francis, D., Stevenson, R.K., 2008. Neodymium-142 evidence for hadean mafic crust. Science 321, 1828–1831.
O'Neil, J., Maurice, C., Stevenson, R.K., Larocque, J., Cloquet, C., David, J., Francis, D., 2007. The geology of the 3.8 Ga Nuvvuagittuq (Porpoise Cove) greenstone belt, northeastern Superior Province, Canada. In: Van Kranendonk, M.J., Smithies, R.H., Bennett, V. (Eds.), Earth's Oldest Rocks. Elsevier, Amsterdam, pp. 219–254.
Papineau, D., Mojzsis, S.J., Coath, C.D., Karhu, J.A., McKeegan, K.D., 2005. Multiple sulfur isotope analyses of sulfides in the aftermath of Paleoproterozoic glaciations. Geochim. Cosmochim. Acta 69, 5033–5060.
Papineau, D., Mojzsis, S.J., Schmitt, A.K., 2007. Multiple sulfur isotopes from Paleoproterozoic Huronian interglacial sediments and the rise of atmospheric oxygen. Earth Planet. Sci. Lett. 255, 188–212.
Perry, E.C., Ahmad, S.N., Swulius, T.M., 1978. The oxygen isotope composition of 3,800 m.y. old metamorphosed chert and iron formation from Isukasia, West Greenland. J. Geol. 86, 223–239.
Roth, A.S.G., Bourdon, B., Mojzsis, S.J., Touboul, M., Sprung, P., Guitreau, M., Blichert-Toft, J., 2013. Inherited ^{142}Nd anomalies in Eoarchean protoliths. Earth Planet. Sci. Lett. 361, 50–57.
Rouchon, V., Orberger, B., 2008. Origin and mechanisms of K–Si-metasomatism of ca. 3.4–3.3 Ga volcaniclastic deposits and implications for Archean seawater evolution: examples from cherts of Kittys Gap (Pilbara craton, Australia) and Msauli (Barberton Greenstone Belt, South Africa). Precambrian Res. 165, 169–189.
Schmitt, A.K., Vazquez, J.A., 2006. Alteration and remelting of nascent oceanic crust during continental rupture: evidence from zircon geochemistry of rhyolites and xenoliths from the Salton Trough, California. Earth Planet. Sci. Lett. 252, 260–274.
Spear, F.S., 1981. An experimental study of hornblende stability and compositional variability in amphibolite. Am. J. Sci. 284, 697–734.
Van Kranendonk, M.J., Hickman, A.H., Smithies, R.H., Nelson, D.R., 2002. Geology and tectonic evolution of the Archean North Pilbara Terrain, Pilbara Craton, Western Australia. Econ. Geol. 97, 695–732.
Whitehouse, M.J., Platt, J.P., 2003. Dating high-grade metamorphism—constraints from rare-earth elements in zircon and garnet. Contrib. Min. Pet. 145, 61–74.
Yamashita, K., Creaser, R.A., Villeneuve, M.E., 2000. Integrated Nd isotopic and U–Pb detrital zircon systematics of clastic sedimentary rocks from the Slave Province, Canada: evidence for extensive crustal reworking in the early- to mid-Archean. Earth Planet. Sci. Lett. 174, 283–299.
Young, E.D., Nagahara, H., Mysen, B.O., Audet, D.M., 1998. Non-Rayleigh oxygen isotope fractionation by mineral evaporation: theory and experiments in the system SiO_2. Geochim. Cosmochim. Acta 62, 3109–3116.